Heliyon 10 (2024) e38301

Contents lists available at ScienceDirect

Heliyon

journal homepage: www.cell.com/heliyon

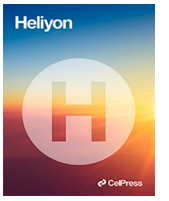

Research article

Single-cell RNA sequencing profiling of mouse cardiac cells in response to retinoic acid

Qianqian Yin [a,b], Qing Chu [a], Haobin Jiang [a], Jie Feng [a], Hong Lian [a], Yu Nie [a,c,*], Shengshou Hu [a,**]

[a] State Key Laboratory of Cardiovascular Disease, Fuwai Hospital, National Center for Cardiovascular Disease, Chinese Academy of Medical Sciences and Peking Union Medical College, Beijing, 100037, China
[b] Center of Basic Medical Research, Institute of Medical Innovation and Research, Peking University Third Hospital, Beijing, 100191, China
[c] National Health Commission Key Laboratory of Cardiovascular Regenerative Medicine, Fuwai Central-China Hospital, Central-China Branch of National Center for Cardiovascular Diseases, Zhengzhou, 450046, China

ARTICLE INFO

Keywords:
Cadiogenesis
Single-cell RNA sequencing
Developmental trajectory
Retinoic acid
Congenital heart disease

ABSTRACT

Congenital heart disease (CHD) is the leading cause of birth defect-related mortality. CHD is a multifactorial, complex disease involving environmental factors playing important roles. To elucidate the cardiac cellular and molecular mechanisms of cardiac malformation, we administered pregnant mice with a single dose of all-trans retinoic acid (RA) at E8.5, as the CHD model. We performed single-cell RNA sequencing on cardiac cells from developing mouse hearts spanning from E8.5 to E17.5 after RA administration. A total of 69,447 cells were obtained from seven developmental stages ranging from E8.5 to E17.5. RA significantly impacted various CM subpopulations, particularly the outflow tract CMs at E9.0 by reduction of Tdgf1 expression. RA also influences the transition of endocardial-to-mesenchymal cells by decreasing the Stmn2 levels, which may contribute to abnormal valve development. In addition, RA altered the metabolic pattern of epicardial cells at E11.5 and promoted its differentiation potential. Taken together, these results are valuable for the development of preventive and therapeutic strategies for CHDs.

1. Introduction

Congenital heart disease (CHD) is a structural defect present at birth that affects the normal function of the heart, which is the

Abbreviations: CHD, congenital heart disease; RA, retinoic acid; TGA, transposition of the great arteries; DORV, double outlet right ventricle; TOF, tetralogy of Fallot; PTA, persistent truncus arteriosus; OFT, outflow tract; CACCT, computer-assisted cardiac cavity tracking; DEGs, differentially expressed genes; scRNA-seq, single-cell RNA sequencing; GO, gene ontology; t-SNE, t-distributed stochastic neighborhood embedding; GSVA, gene set variation analysis; V_CMs, ventricular cardiomyocytes; A_CMs, atrial cardiomyocytes; ECs, endocardial cells; VECs, vascular endocardial cells; SMCs, smooth muscle cells; EPs, epicardial cells; MCs, mesenchymal cells; FBs, fibroblasts; ICs, immune cells.

* Corresponding author. State Key Laboratory of Cardiovascular Disease, Fuwai Hospital & Cardiovascular Institute, National Center for Cardiovascular Disease, Chinese Academy of Medical Science & Peking Union Medical College, 167 Street, Beilishi Road, Xicheng District, Beijing, 100037, China.

** Corresponding author. State Key Laboratory of Cardiovascular Disease, Fuwai Hospital & Cardiovascular Institute, National Center for Cardiovascular Disease, Chinese Academy of Medical Science & Peking Union Medical College, 167Street, Beilishi Road, Xicheng District, Beijing, 100037, China.

E-mail addresses: nieyu@fuwaihospital.org (Y. Nie), huss@fuwaihospital.org (S. Hu).

https://doi.org/10.1016/j.heliyon.2024.e38301
Received 6 March 2024; Received in revised form 28 August 2024; Accepted 20 September 2024
Available online 23 September 2024

leading cause of mortality from birth defects worldwide with 13.3 million patients globally in 2019 [1]. There has been a global transition in the age distribution of deaths from the pediatric to adult populations [2]. CHD has become the leading cause of death from non-communicable diseases in populations under 20 years old [3]. Conotruncal defects, which result from abnormal development of the conotruncus in the early stages of heart development, account for approximately 30 % of all CHDs. These include transposition of the great arteries (TGA), double outlet right ventricle (DORV), tetralogy of Fallot (TOF), persistent truncus arteriosus (PTA), pulmonary atresia, and other malformations. Despite significant advancements in diagnostic and therapeutic techniques, CHD remains a major cause of infant morbidity and mortality. There is a need to better understand the molecular characteristics of CHD to better formulate effective prevention and intervention strategies.

Single-cell RNA sequencing (scRNA-seq) has provided unprecedented resolution for the study of complex heart developmental and disease processes [4–10]. Studies using scRNA-seq of human and murine hearts have revealed the well-characterized anatomical features and mechanisms of cardiogenesis. Moreover, scRNA-seq can identify previously unrecognized populations of disease-associated cells or functional states as well as potential molecular regulators of heart disease-associated processes [11,12]. Single-cell transcriptomics technology has well-studied the transcriptional characteristics of congenital heart disease caused by genetic factors, such as NKX2-5 [13], Hand2 [11], WT1 and Tbx18 [8]. Besides that, the maternal metabolic environment also plays a crucial role in embryonic heart development. Retinoic acid (RA) signaling plays a critical role in heart development. Excess RA acts as a teratogen can cause abnormal heart development and CHD, mainly by affecting the outflow tract (OFT) and leading to conditions such as TGA, DORV, TOF, and PTA. These observations closely resemble conotruncal heart defects caused by RA treatment in pregnant women [14]. The importance of retinoic acid in embryonic development makes this model more reflective of certain mechanisms of congenital heart disease in humans. Therefore, the RA-induced CHD model is suitable for investigating the mechanisms underlying CHD in the maternal metabolic environment [15–17]. scRNA-seq is particularly well-suited for analyzing cellular heterogeneity, dynamic behaviors, and transcriptional regulation changes during abnormal cardiac morphogenesis in the context of teratogens.

Based on an RA-induced CHD mice model, this study employed scRNA-seq to build a cellular landscape of RA-induced cardiac malformation. A total of 69,447 cells from seven developmental stages spanning from E8.5 to E17.5 were obtained. Our extensive analysis found that excess RA changed gene expression during cardiac cell development. Our scRNA-seq dataset and the associated transcriptional features are valuable for the development preventative and therapeutic strategies for CHDs.

2. Results

2.1. Embryonic cardiac cell landscape with RA treatment by single-cell RNA sequencing

To investigate the effect of RA on early cardiac development, we successfully established a model of conotruncal defects in CD1 mice as previously described [15,17]. Briefly, pregnant mice were administered a single dose of all-trans RA (160 mg/kg b.w., Sigma) at E8.5 (Fig. 1A). We observed a shortened outflow tract (OFT) in RA-treated embryos at E9.0 (Fig. 1B). Conotruncal defects were observed in 70 % of embryonic hearts at E17.5, as determined using acomputer-assisted cardiac cavity tracking (CACCT) system [17] (Table S1 and Fig. 1C).

To systematically investigate the cellular heterogeneity and transcriptomic dynamics during mouse embryonic heart development following RA treatment (with corn oil treatment as the control), we collected embryonic mouse hearts at various developmental stages: E8.5, E9.0, E9.5, E10.5, E11.5, E14.5, and E17.5. The hearts were digested into a cell suspension (Fig. 1D). Single-cell gene expression profiles were obtained using a Chromium system (10x Genomics), resulting in 69,447 individual cells after stringent filtration (Table S2). These cells were assigned to 26 clusters using t-distributed stochastic neighborhood embedding (t-SNE) analysis with Seurat 4.1.1 (Fig. 1E and Fig. S1A). Based on well-known cell-type-specific markers [4,5] and cluster marker genes (Fig. 1F and Fig. S1B), we identified eight major cell types (Fig. 1E), including ventricular CMs (V_CMs, Myl2) and atrial CMs (A_CMs, Nr2f1), endocardial cells (ECs, Cdh5), vascular endocardial cells (VECs, Npr3), smooth muscle cells (SMCs, Acta2), epicardial cells (EPs, Wt1), mesenchymal cells (MCs, Sox9), fibroblasts (FBs, Pdgfra), and immune cells (ICs, C1qa).

To understand the dynamics of cell type composition during embryonic heart development in response to RA, we calculated the proportions of each cell type at each time point (Fig. 1G and Fig. S1C). The results revealed proportional changes in each cell type, indicating a progressive increase in cellular complexity throughout embryonic heart development. During normal development, CMs and ECs were the predominant cell types at E8.5 and E9.0, whereas EPs and MCs were predominantly detected at E9.5 and E11.5. FBs, VECs, and SMCs were mainly detected at E14.5-E17.5. RA seems not exhibit any significant alterations in major cell type composition. ECs showed a slight decrease at E9.0 after RA treatment.

2.2. Effects of excess RA on subpopulations of cardiomyocytes development

As shown in our scRNA-seq data, cardiomyocytes represented the largest proportion of cells. We reconstructed the developmental time course of cardiomyocytes in the control group using Monocle 2 and identified five major categories of transcriptional gene clusters with distinct patterns (Fig. S2A). Based on GO analysis, genes in clusters G1, G2, and G5 were enriched in "cell cycle," "translation," and "ribosome biogenesis,", indicating a more proliferative state of cardiomyocytes at the early time points. Conversely, genes in clusters G3 and G4 displayed a gradually increasing trend. They were enriched in "muscle structure development," and "oxidative phosphorylation," respectively, indicating a more mature state of cardiomyocytes at later time points than at earlier time points. Furthermore, we used these gene sets to evaluate the effect of RA on CMs and we found that RA affected energy metabolism, proliferation and muscle development (Fig. S2B). This result suggested that RA influences various aspects of cardiomyocyte

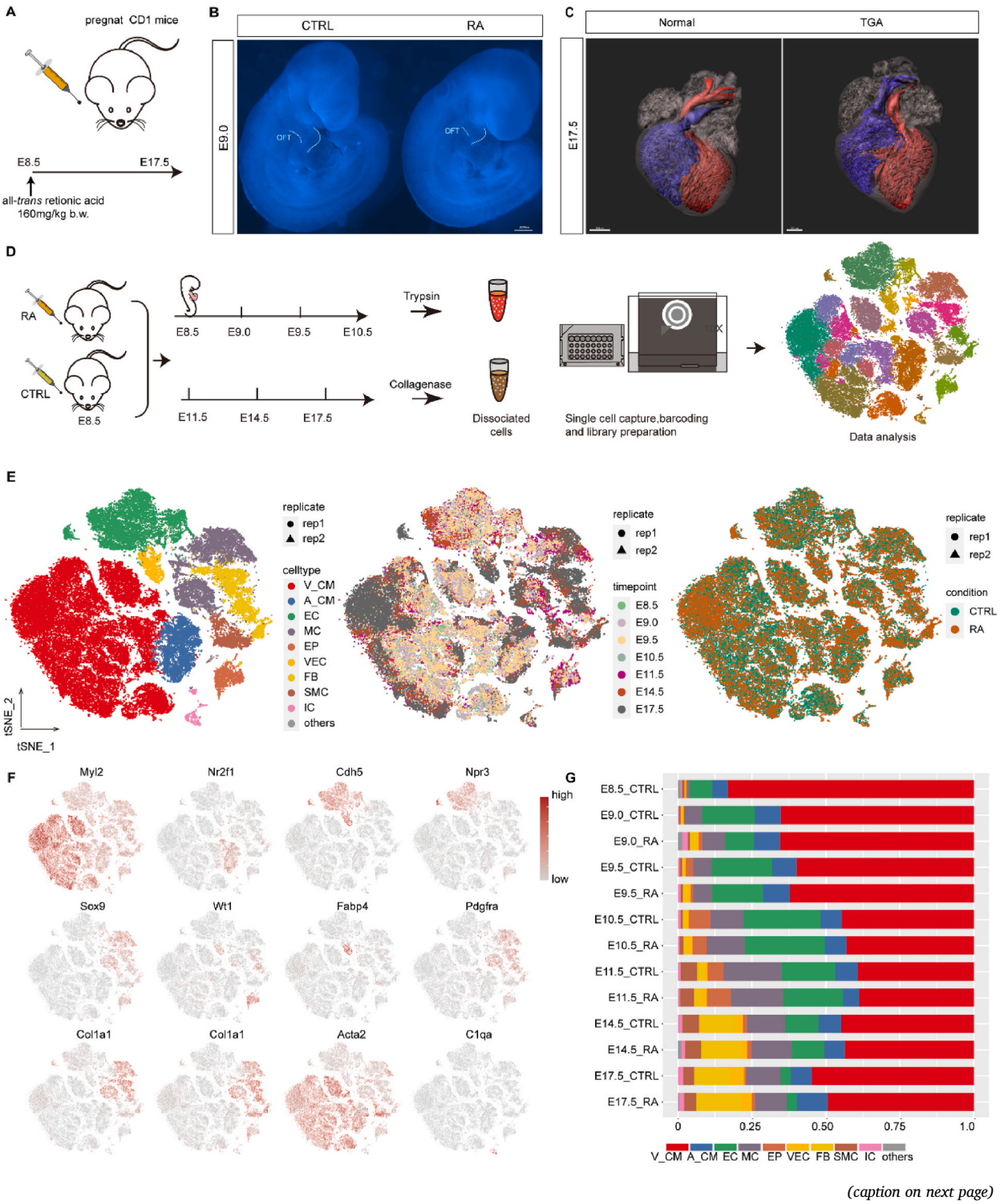

(caption on next page)

Fig. 1. Single-cell transcriptome analysis of the mouse embryonic heart development under retinoic acid (RA) treatment. (A) Schematic representation of the congenital heart disease mice model construction.CTRL: corn oil treatment, RA: retinoic acid treatment. (B) Shorted outflow tract (OFT) length was detected in RA-treated embryos at E9.0. scale bar: 2000 μm. (C) The phenotype of heart at E17.5 induced by RA. TGA: transposition of the great arteries. scale bar: 300 μm. (D) Schematic representation of the experimental procedure for preparation of cardiac cell preparation for single-cell RNA-seq analysis. RA: retinoic acid treatment, CTRL: corn oil treatment. (E) t-distributed stochastic neighbor embedding (t-SNE) plots of mouse embryo cardiac cell clusters, timepoints and conditions. Clusters, conditions and time points are shown in different colors. ventricular cardiomyoytes (V_CMs), atrial cardiomyoytes (A_CMs), endocardial cells (ECs), vascular endocardial cells (VECs), smooth muscle cells (SMCs), epicardial cells (EPs), immune cells (ICs), mesenchymal cells (MCs), fibroblasts (FBs). (F) t-SNE projection of cells and typical gene expressions. (G) Proportion of cell types per sample with or without RA treatment. (For interpretation of the references to color in this figure legend, the reader is referred to the Web version of this article.)

development.

We performed a re-clustering analysis of the cardiomyocytes and identified nine distinct cell clusters (Fig. 2A and Fig. S2C). Based on gene marker analysis and GO analysis (Fig. 2B–C and Fig. S2D), we identified proliferation CMs (cluster 0 and 6) expressed Mki67 and Ccnb2 associated with cell proliferation; A_CMs (cluster 1) expressed Nr2f1, Sln and Nr2f2, which marked atrial CMs; outflow tract CMs (OFT_CMs, cluster 4) expressed Tnc and Bmp4; atrioventricular canal-specific CMs (AVC_CMs, cluster 7) expressed Rspo3; Mb^{+} CMs that highly expressed Mb (cluster 2), $Prmt1^{+}$ CMs that highly expressed Prmt1 (cluster 3), and $Slit2^{+}$ CMs (cluster 5) that highly expressed Slit2. Proliferation CMs, Mb^{+}, $Prmt1^{+}$, and $Slit2^{+}$ CMs were ventricular CMs (V_CMs). To study the effect of RA on CM subpopulations gene expression, we analyzed differential gene expression in each cardiomyocyte subpopulation at different time points (Fig. 2D). The cell subtype with the largest number of differentially expressed genes (DEGs) was the $Prmt1^{+}$ CMs (cluster 3) at E17.5, followed by the OFT_CMs (cluster 4) at E9.0. Scoring the cells using gene set G1-G5, RA-regulated genes, and CHD-related genes, we found that Cell proliferation and oxidative phosphorylation score decreased, and RA signaling score increased in OFT_CMs at E9.0 (Fig. 2E). These results suggested that excess RA induced RA signaling pathway, and affected cell proliferation, metabolic pattern in OFT_CMs at earlier timepoint. Meanwhile, the muscle structure development score and CHD score increased in $Prmt1^{+}$ CMs at E17.5 (Fig. 2F), suggesting that $Prmt1^{+}$ CMs may play a significant role in the cardiac remodeling associated with the TGA phenotype. We also have conducted the analysis on $Slit2^{+}$ CMs at E11.5, which is the time point when $Slit2^{+}$ CMs are most affected. The upregulated genes were enriched in metabolic process and downregulated genes were enriched in heart morphogenesis (Figs. S2E and F). These findings indicate that RA affects cardiomyocyte subpopulations metabolic patterns may be involving in heart morphogenesis.

Excess RA acts as a teratogen during development and can cause abnormal heart development and CHD, particularly affecting the OFT. OFT_CMs is dramatically affected at E9.0 which seems to more sensitive to RA (Fig. 2D). We analyzed differential gene expression in OFT_CMs at E9.0 and E9.5 (Fig. 3A–B). At E9.0, 12 h after RA treatment, we observed significant upregulation of Cyp26a1, an enzyme involved in RA metabolism. In addition, Tbx20, Rspo3, and Tdgf1 were downregulated by RA, whereas Mdk and Cck were upregulated. GO analysis showed that genes downregulated at both E9.0 and E9.5 were enriched in outflow tract development and neural crest cell development (Fig. 3C). In contrast, upregulated genes were enriched in cardiac chamber morphogenesis, muscle cell development, and glucose metabolism (Fig. S3). Immunofluorescence staining confirmed the decrease in Tdgf1 expression (Fig. 3D). These results suggested that RA treatment affects outflow tract development which may related to Tdgf1 reduction.

At E17.5, when transposition of the great arteries (TGA) had already occurred. We analyzed the differential gene expression in $Prmt1^{+}$ CMs (Fig. 3E). GO analysis of the differentially expressed genes indicated that the upregulated genes were primarily enriched in muscle cell differentiation and muscle cell development (Fig. 3F). In contrast, the downregulated genes were mainly enriched in energy metabolism, such as oxidative phosphorylation (Fig. 3G). These results suggested that RA affected $Prmt1^{+}$ CMs energy metabolism in TGA.

2.3. Effects of excess RA on ECs and MCs development

Considering that the endocardial-to-mesenchymal transitions (EndoMT) is a key process in outflow tract formation, we refined the clustering analysis among cardiac ECs and MCs to study cellular heterogeneity under RA treatment (Fig. 4A–B and Figs. S4A–B). We found that Cluster 4 highly expressed Ccdc141, Aqp1, and Klf2, which consisted of EC and MC, predominantly obtained from E8.5-E11.5 (Figs. S4A–D). The highly expressed genes were enriched in "regulation of vasculature development," "vasculogenesis," and "heart morphogenesis" (Figs. S4E–F). These results indicated that this cluster may be related to EndoMT. We re-clustered cluster 4, which possessed the potential to transition into mesenchymal cells, into three clusters (Fig. 4 C). The upregulation of Cyp26a1 and Cyp26b1 indicated the influence of RA (Figs. S4G–H). C4-0 highly expressed Stmn2, C4-1 highly expressed Sox9, and C4-2 highly expressed Cav1 (Fig. 4D–E). To recover the gene expression dynamics that characterize EndoMT progression, we ordered the cells to build a pseudotemporal trajectory (Fig. 4 F and Fig. S5). We found that the development of endocardial cells into mesenchymal cells followed a continuum program and pseudotime ordering closely matched the graph-based clustering results. C4-0 was isolated centrally along this differentiation axis, supporting the notion that C4-0 is an intermediate transition state between ECs and MCs. We identified Stmn2, a neuronal growth-associated protein involved in neuronal differentiation, as a specific marker of this subtype and verified it by immunofluorescence (Fig. 4G). The expression levels of the Nrp1 decreased in the endocardial region over the pseudospatial trajectory and the expression levels of Limd2 increased sharply in mesenchymal cells. Stmn2 and Pdlim3, which are reported to influence cancer metastasis by promoting epithelial-to-mesenchymal transition [18], were specifically expressed in C4-0 cells (Fig. S6G), suggesting they may play an important role in EndoMT.

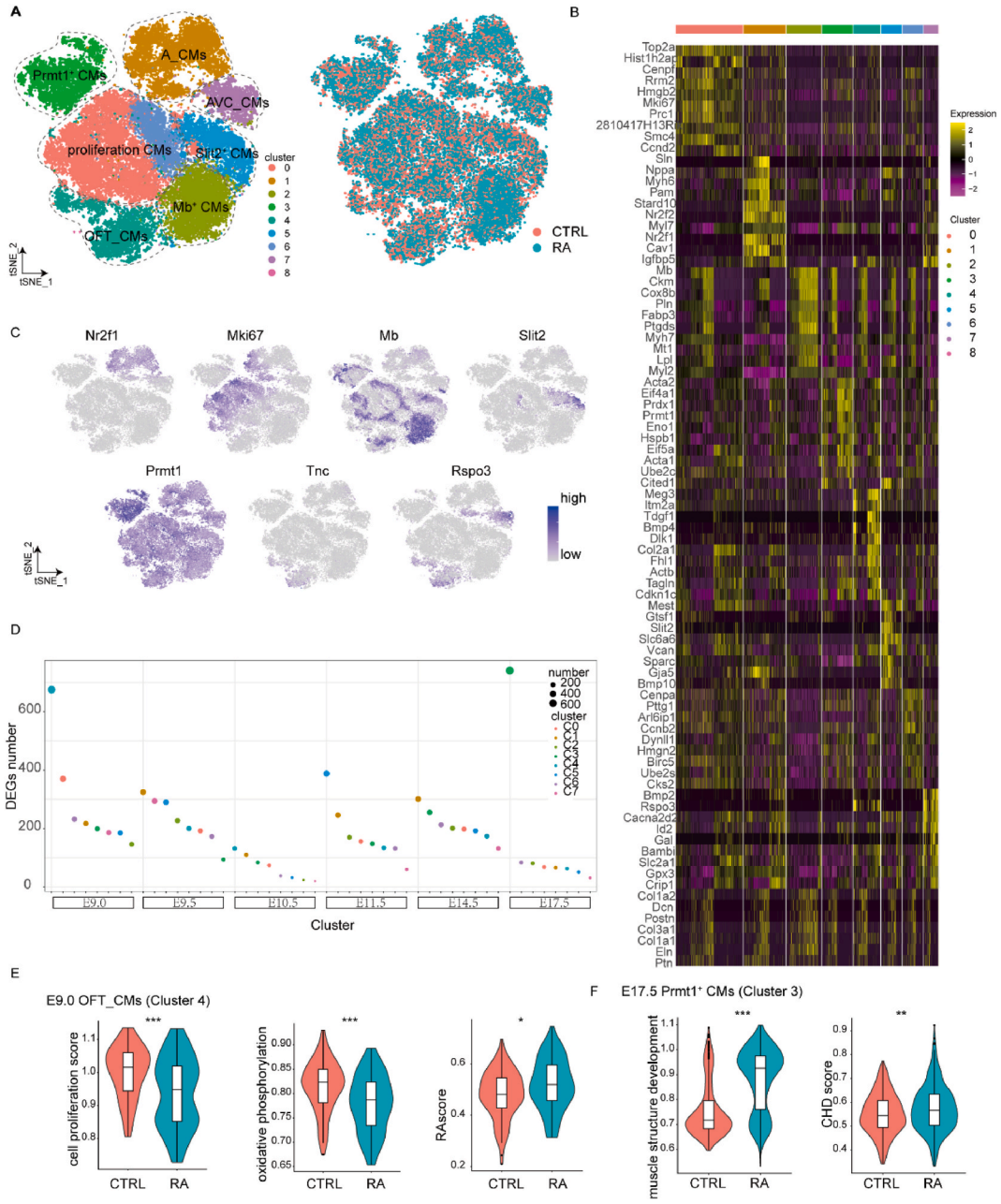

Fig. 2. Excess RA disturbed cardiomyocytes development. (A) t-distributed stochastic neighbor embedding (t-SNE) plots of mouse embryo cardiac CM subpopulations by cluster (left) and condition (right). (B) heatmap of marker genes of CM subpopulations. (C) Featureplot of representing gene expressions. (D) the number of DEGs of RA treatment in clusters during different time point. (E) cell proliferation, oxidative phosphorylation score reduced and RA signaling score increased in cluster 4 in E9.0. (F) muscle structure development score and CHD score increased in cluster 3 in E17.5.

We analyzed the differential gene expression in C4-0 and C4-1obtained from E9.0-E11.5. We found that Stmn2, Tbx20, and Twist1 expression decreased in C4-0 after RA treatment. Spint2 levels increased, S100a4 and Sox9 levels decreased in C4-1 after RA treatment (Fig. 4H). The decreased Sox9 was verified by immunofluorescence (Fig. 4I). GO analysis revealed that RA promoted glycolysis and ATP generation (Fig. 4J). These results suggested that RA reduced Stmn2 level in cells at intermediate transition state to disturb EndoMT, which may explain the cardiac valve defect.

2.4. Molecular characteristics of epicardial cells development after RA treatment

To further characterize the EPs populations which is important for heart development in RA-treated and control hearts, we re-

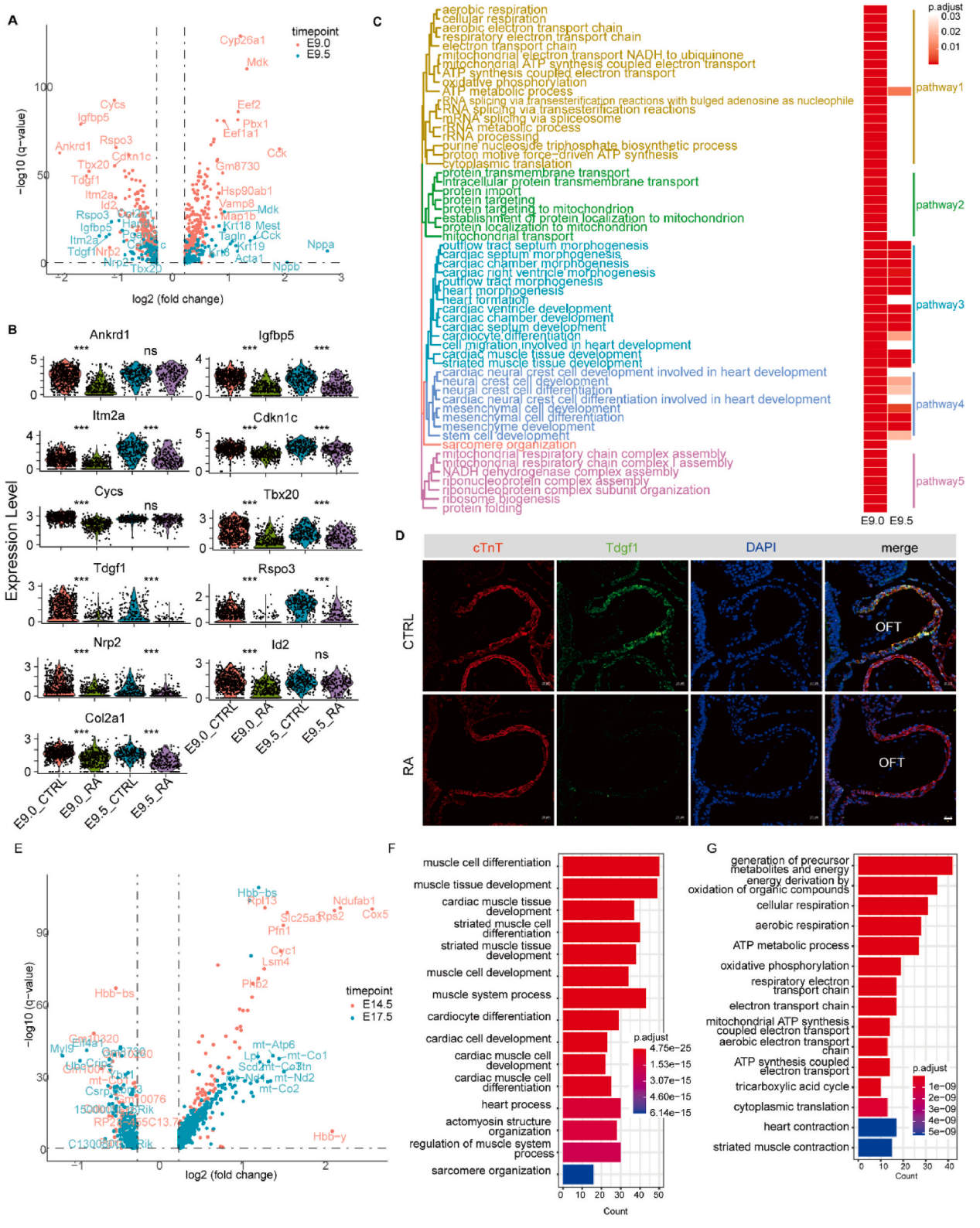

(caption on next page)

Fig. 3. Retinoic acid induced CM subpopulation dysregulated gene expression. (A) Volcano plot displaying the differentially expressed genes (DEGs) of outflow tract CMs (OFT_CMs) between the control and RA-treated cells at E9.0 and E9.5. (B) Vlnplot of differential expression of representative genes. Significance was assessed compared with the controls using wilcoxon rank sum test. ***: $P < 0.001$, ns: no significance. (C) Gene ontology (GO) analysis of downregulated genes of OFT_CMs at E9.0 and E9.5. (D) Immunofluorescence for Tdgf1 and cTnT at E9.0. OFT: outflow tract. scale bar: 20 μm (E) Volcano plot displaying the DEGs of cluster 3 between the control and RA-treated cells at E14.5 and E17.5. (F) GO analysis of upregulated genes of cluster 3 at E17.5. (G) GO analysis of downregulated genes of cluster 3 at E17.5.

analyzed the EPs. EPs were clustered into two subpopulations that showed a temporal distribution despite removing batch effects using harmony (Fig. 5A–B and Fig. S6A). Cluster 0 mainly consisted of cells from E9.0 to E11.5, which showed characteristics distinct from Cluster 1, primarily included cells from E11.5 to E14.5 (Figs. S6B–D). EPs with high stemness were enriched in Cluster 0 (Fig. 5C and Fig. S6E). The epicardium is also a progenitor cell type, and Cluster 0 exhibited a higher differentiation potential. We found that only the E11.5 time point included cells from both clusters (Fig. 5D), indicating that epicardial cells start to differentiate at this time point. However, RA significantly promoted the differentiation potential of EPs at E11.5 (Fig. S6E).

To further investigate the differences between these two cell populations, we performed a differential analysis of Cluster 0 and Cluster 1 of E11.5 (Fig. 5E).We found that Cluster 0 showed high expression of cell proliferation genes enriched in proliferation-related biological processes. Genes highly expressed in Cluster 1 were enriched in the extracellular matrix and extracellular structure organization (Fig. 5F). We examined the effects of RA on EPs subpopulations using differential analysis. In cluster 0, RA promoted glucose metabolism in the proliferative epicardial cells, reducing steroid metabolism, extracellular matrix, and cell proliferation (Fig. 5G, upper). In cluster 1, RA promoted glucose metabolism and downregulated extracellular matrix, suggesting a significant effect of RA on cell metabolism (Fig. 5G, bottom). We also conducted scMetabolism analysis and found that RA influenced metabolism at E11.5. RA promotes glycolysis and pyruvate metabolism. These results indicated that glucose metabolism is the important energy metabolism pattern of Eps after RA treatment.

3. Discussion

Here, we present scRNA-seq data on 69,447 cardiac cells from control and RA-treated hearts spanning seven developmental stages between E8.5 and E17.5. In addition to characterizing the molecular features of different cell types, we established developmental cardiac cellular profiles in an RA-induced CHD model and identified cardiac cell cellular and molecular dynamics under ectopic RA signaling.

The maternal metabolic environment plays a crucial role in embryonic heart development. RA signaling affects the patterning of cardiac progenitors and can cause a spectrum of congenital anomalies, especially OFT and septal defects, in mice. Using the RA-induced CHD model, the extensive effects of RA also changed the cellular molecular characteristics. As the most abundant cell type captured, CMs subpopulations showed different susceptibility to RA. At E9.5, OFT-CMs were affected dramatically by excess RA signaling. We found that RA reduced Tdgf1 levels of OFT-CMs. Tdgf1 is a direct transcriptional target of Mef2c in OFT alignment [19]. The reduction of Tdgf1levels in OFT-CMs may be responsible for OFT shortening, which may be the main reason for conotruncal malformations. This observation is similar to the loss of Hand2 resulting in disrupted OFT-fated cell specification [11]. At the molecular level, RA downregulated genes in OFT-CMs enriched in the GO terms ‘cardiac chamber morphogenesis’ and ‘outflow tract morphogenesis.’ We observed that the upregulated genes in OFT-CMs were enriched for the GO term “muscle cell contraction,” which may indicate that RA impaired myocardial cell shape related to OFT malformation [20,21]. At E11.5, Slit2$^+$ CMs undergone significant transcriptional changes. The upregulated genes were enriched in metabolic process and downregulated genes were enriched in heart morphogenesis. After TGA formation, the muscle structure development score and CHD score increased in Prmt1$^+$ CMs at E17.5, suggesting that Prmt1$^+$ CMs may play a significant role in the cardiac remodeling.

We analyzed heterogeneity and lineage relationships among endothelial cells during EndoMT. Our data revealed that Stmn2, a protein that regulates neuronal growth, was enriched in ECs with the potential to differentiate into MCs. Loss-of-function studies have shown that abnormal EndoMT (resulting in deficient or excessive OFT cushion formation) can lead to structural OFT defects [22], particularly alignment defects. RA reduced Stmn2 level in cells at intermediate transition state between ECs and MCs during EndoMT. Morever, Some signaling molecules (Tbx20 and Twist1) required for EndoMT in endocardial cushion development were down-regulated, indicating that the activation of endothelial cells lining the OFT region was affected. We also found S100a10, which is reported to promote cancer cell proliferation, migration and invasion [23], were also decreased at E9.0 and E9.5. Further studies need to reveal the role of S100a10 in EndoMT. Moreover, at E9.0, the down-regulated genes involved in EndoMT, which affects cardiac cushion development, may be responsible for the decrease in MCs at E9.5. These results indicate that cardiac cushion development was disrupted, which may be one of the reasons for conotruncal malformation.

EPs involved in the formation of the heart’s structure could migrate into the myocardium through differentiate into different cell types. This plasticity is vital for the proper formation of the heart and its associated structures. In our study, the EPs at earlier time point were distinct from EPs at later time point. We found that E11.5 is an important time point when epicardial cells start to differentiate. However, EPs’ plasticity was affected for that the differentiation potential increased at E11.5 after RA treatment. Moreover,we found that RA influences the metabolic patterns of a subset of cells with stem-like properties. It seems that glucose metabolism is the important energy metabolism pattern of EPs after RA treatment. Whether the metabolic patterns changes are related to its plasticity should be further studied.

However, the study has several limitations. Our datasets may be constrained regarding replication, sampling regions, lineage

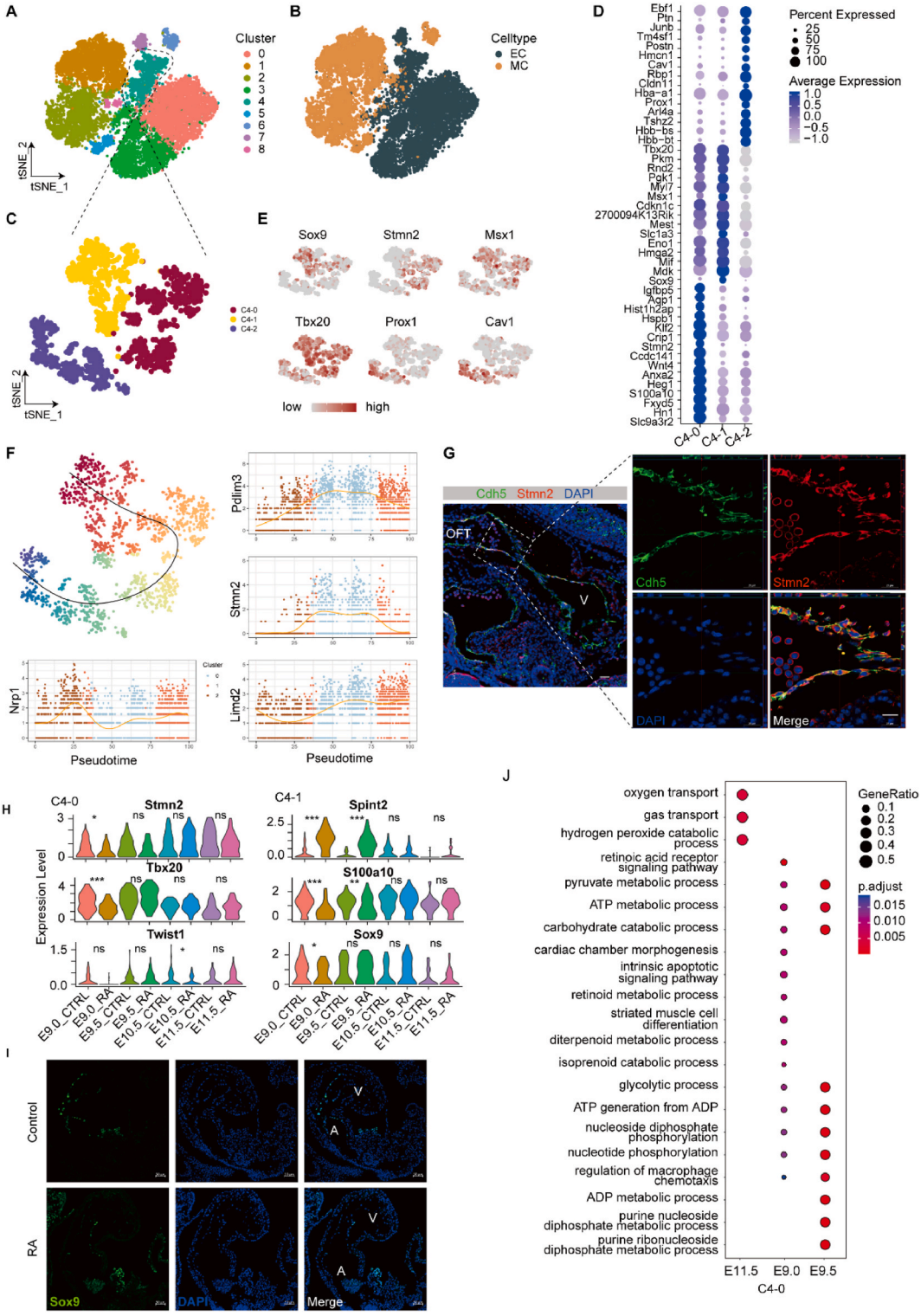

Fig. 4. The molecular features of endocardial cells (ECs) and mesenchymal cells (MCs) under ectopic RA treatment. (A–B) t-SNE showing the re-clustering of control and RA-treated ECs and MCs. **(C)** t-SNE showing the re-clustering of cluster 4 in Fig. 4A. (D) Dotplot of clusters marker genes. (E) Featureplot of representative genes expression. (F) Pseudotime trajectory and representative genes expression. (G) Immunofluorescence for STmn2 in control and RA-treated embryos at E9.5. scale bar: 20 μm (H) Vlnplot of representative genes expression. *: $P < 0.05$, **: $P < 0.01$, ***: $P < 0.001$, ns: no significance. **(I)** Immunofluorescence for Sox9 in control and RA-treated embryos at E9.0. A: atrium. V: ventricle. scale bar: 50 μm (J) GO analysis of upregulated genes of cluster 0 (C4-0) under RA treatment.

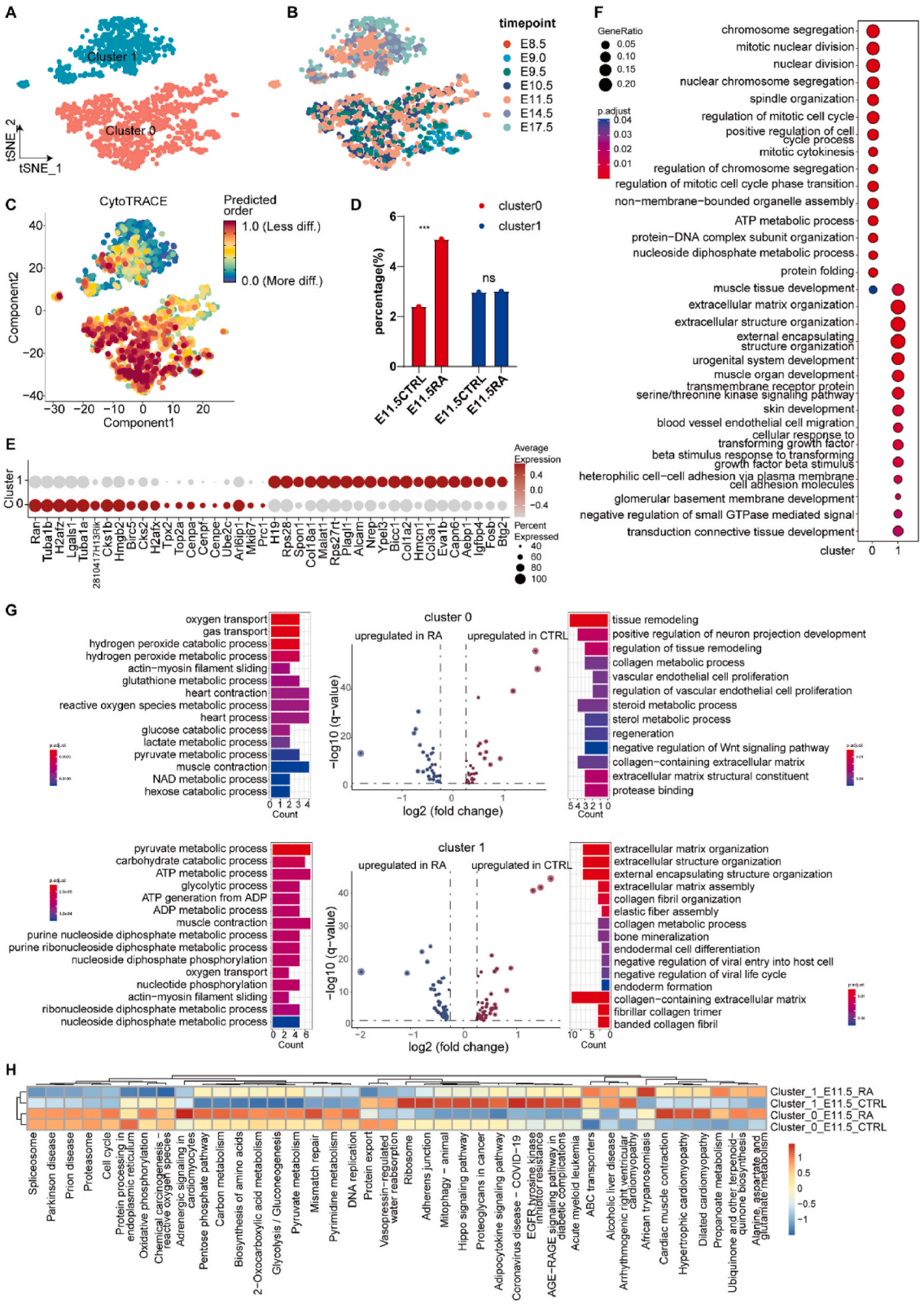

(caption on next page)

Fig. 5. EPs were affected by ectopic RA. (A) t-SNE showing the second-level clustering of control and RA-treated EPs by cluster and timepoint **(B)**. **(C)** t-Distributed Stochastic Neighbor Embedding (tSNE) depicting the distribution of CytoTRACE scores among EPs. Dark-green indicates lower scores (low stemness) while dark-red indicates higher scores (high stemness). **(D)**Percentage of cluster 0 and 1 in control and RA-treated group at E11.5. ***: ***P*<0.001(E)** Dotplot of clusters marker genes of Eps at E11.5. **(F)** GO analysis of marker genes of clusters at E11.5. **(G)** GO analysis of upregulated (upper) and downregulated genes (bottom) of cluster 0 at E11.5. **(H)** Gene set variation analysis (GSVA) showed the effect of RA on subclusters of EPs at E11.5. (For interpretation of the references to color in this figure legend, the reader is referred to the Web version of this article.)

tracing of progenitor cells, and the lack of anatomical region information. In addition, the lack of experimental validation for some results is a significant limitation, necessitating further experimental verification to fully understand how dysregulated genes induced by RA contribute to heart defects.

Overall, employing single-cell RNA-seq, we constructed embryonic cardiac cell developmental trajectories spanning E8.5 and E17.5 and revealed the spatiotemporal dynamics of regulatory network of cardiogenesis. Excess RA induced ectopic RA signaling and disrupted the CM subpopulations, EndoMT and EPs development. These results are valuable for developing preventative and therapeutic strategies for the broad etiology of CHDs in the further.

4. STAR★Methods

4.1. Mouse model

Pregnant CD1 mice (female, 8–10 weeks old) were obtained from SPF Biotechnology Co., Ltd and housed under specific pathogen-free conditions. To generate a congenital heart disease mouse model, pregnant females were administered a single oral dose of all-trans retinoic acid (160 mg/kg b.w., Sigma) dissolved in corn oil (Sigma) on embryonic day 8.5. Pregnant mice administered corn oil (160 mg/kg b.w., Sigma) via oral gavage was used as controls. Cardiac malformations in mouse embryos were assessed on embryonic day 17.5 using a computer-assisted cardiac cavity tracking system (CACCT).

4.2. Mouse embryonic heart collection and single-cell preparation

To prepare single cells for RNA-seq, CD1 mouse embryonic whole hearts at embryonic days (E) 8.5, E9.0, E9.5, E10.5, E11.5, E14.5 and E17.5 were excised into PBS under a stereo microscope (V8, Carl Zeiss). Hearts collected from one pregnant mouse were pooled together. Two embryonic hearts were collected at E11.5. At E14.5 and E17.5, one embryo heart was collected and its phenotype was identified under a stereo microscope. Samples from E8.5, E9.0, E9.5, and E10.5 were digested into single cells with 0.25 % trypsin-EDTA incubated at 37 °C with gentle shaking every 2–3 min, depending on stages. Samples from E11.5, E14.5, and E17.5 were digested into single cells with a Neonatal Heart Dissociation Kit (Miltenyi Biotec) incubated for 20–40 min at 37 °C with gentle shaking every 10 min. Single-cell suspensions were filtered through a 70 μm filter to remove residual undigested tissue pieces, centrifuged at 200 g for 3 min, and resuspended at 1×10^6 cells per milliliter in PBS with 0.04 % bovine serum albumin (Sigma) for single-cellRNA sequencing.

4.3. Single-cell RNA sequencing and data processing

Cardiac cell count and viability were determined using trypan blue staining by Automated Cell Counter (Countstar® BioTech). Cells from each time point were loaded for capture onto the Chromium System using the Chromium Single Cell 3′ Reagent Kits v2 (10X Genomics). Following capture and lysis, cDNA was synthesized and amplified according to the manufacturer's instruction (10X Genomics). The amplified cDNA from each channel of the Chromium System was used to construct a sequencing library and sequenced on on a HiSeq X10 (Illumina) with a paired end of 150 bp. Each litter's control and RA-treated replicate libraries were pooled and sequenced in the same lane.

Cell Ranger v1.3 (10X Genomics) was used to process raw sequencing data and generate gene expression matrix files. We performed further filtering and clustering analyses of these cells using R software (version 4.2.1) and Seurat (version 4.1.1). As a further quality-control measure, we filtered out doublets that were perceived on the basis of the DoubletFinder package (version 2.0.3). Cells with $<$400 unique genes expressed, or $>$25 % of the reads mapped to mitochondria were filtered. The integrated data were normalized (NormalizeData), scaled (ScaleData). Harmony software (version 0.1.0) was used to correct for the batch effects. Downstream graph-based clustering into distinct populations using the FindClusters function, and t-distributed stochastic neighborhood embedding (t-SNE) dimensionality reduction were used to project these populations in two dimensions. We removed blood clusters based on the expression of known blood markers, such as the hemoglobin genes (*Gypa* and *Hba-a2*) and repeated the clustering approach for these retained cells, as mentioned above. Differentially expressed genes (DEGs) were identified among the clusters in Seurat using the FindAllMarkers function (Wilcoxon rank-sum test) to identify the marker genes. Genes with the log-fold change $|\text{logFC}| \geq 0.25$ and false discovery rate (FDR) < 0.05 were considered significant. Cell proportion was calculated using the speckle package [24]. We used the Gene Set Variation Analysis (GSVA) enrichment to obtain Hallmark gene set (MSigDB) scores through the R package GSVA (version 1.44.2). Gene Ontology (GO) gene enrichment analysis was conducted using the ClusterProfiler package (version 4.4.4). The R package scMetabolism (version 0.2.1) evaluated metabolic activity using mouse Kyoto Encyclopedia of Genes and Genomes pathways built based on Kyoto Encyclopedia of Genes and Genomes (https://www.genome.jp/kegg/).We calculated cell scores using the

"AddModuleScore" function in the Seurat package with default parameters. Cell Proliferation scores were computed using G1, G2, and G5 (Table S3). RA response score used previously reported RA regulated gene sets [25]. CHD score used gene reported associated with CHD [26].The Monocle 2 package was used to analyze single-cell trajectories and identify developmental transitions. R package CytoTRACE v0.3.3 was applied to calculate the CytoTRACE [27] scores for the EPs. CytoTRACE scores range from 0 to 1, with higher scores indicating higher stemness (less differentiation), and vice versa.

4.4. Immunofluorescent staining

Hearts were fixed in 4 % PFA overnight at 4 °C, dehydrated in a serial ethanol, xylene, and embedded in paraffin (Thermo Scientific). Thin 40 - μm cryosections were collected using a Leica CM3050S cryostat. For immunohistochemistry, heat-induced antigen retrieval was performed using ethylenediaminetetraacetic acid (EDTA). The sections were incubated with primary antibody overnight at 4 °C. After washing three times with phosphate-buffered saline (PBS), the slides were incubated with appropriate fluorescence-labeled secondary antibodies for 1 h at room temperature. Binding was visualized using Alexa Fluor 488, 594, or 647 fluorophore-conjugated secondary antibodies (Life Technologies). Cell nuclei were stained using DAPI (Life Technologies).

Ethics approval

All animal experiments conducted in this study were approved by the Institutional Animal Care and Use Committee of Fuwai Hospital National Center for Cardiovascular Disease, Chinese Academy of Medical Sciences, and Peking Union Medical College (FW-2021-0044).

Consent for publication

All authors have given their consent for publication of this manuscript.

Data availability statement

Single cell RNA sequencing data were deposited at the Beijing Institute of Genomics (BIG) Data Center (https://bigd.big.ac.cn/) under the accession number CRA002015.

CRediT authorship contribution statement

Qianqian Yin: Writing – review & editing, Writing – original draft, Methodology, Formal analysis. **Qing Chu:** Methodology. **Haobin Jiang:** Methodology. **Jie Feng:** Data curation. **Hong Lian:** Methodology. **Yu Nie:** Writing – review & editing, Supervision, Funding acquisition. **Shengshou Hu:** Supervision, Funding acquisition, Conceptualization.

Declaration of competing interest

The authors declare the following financial interests/personal relationships which may be considered as potential competing interests:YU NIE reports financial support was provided by National Natural Science Foundation of China. If there are other authors, they declare that they have no known competing financial interests or personal relationships that could have appeared to influence the work reported in this paper.

Acknowledgments

This work was supported by the National Key Research and Development Project of China (2019YFA0801500), the Chinese Academy of Medical Sciences (CAMS) Innovation Fund for Medical Sciences (CAMS-I2M, 2021-I2M-1–072), the National Natural Science Foundation of China (8210022095, 81970243, 81770308), National Basic Research Program of China (973 Program, 2010CB529508), and the Beijing Natural Science Foundation (7172183, 7182140).

Appendix A. Supplementary data

Supplementary data to this article can be found online at https://doi.org/10.1016/j.heliyon.2024.e38301.

References

[1] G.A. Roth, et al., Global burden of Cardiovascular diseases and Risk factors, 1990-2019: Update from the GBD 2019 study, J. Am. Coll. Cardiol. 76 (2020) 2982–3021, https://doi.org/10.1016/j.jacc.2020.11.010.

[2] Z. Su, et al., Global, regional, and national time trends in mortality for congenital heart disease, 1990-2019: an age-period-cohort analysis for the Global Burden of Disease 2019 study, EClinicalMedicine 43 (2022) 101249, https://doi.org/10.1016/j.eclinm.2021.101249.
[3] Collaborators, G. B. D. C. H. D., Global, regional, and national burden of congenital heart disease, 1990-2017: a systematic analysis for the Global Burden of Disease Study 2017, Lancet Child Adolesc Health 4 (2020) 185–200, https://doi.org/10.1016/S2352-4642(19)30402-X.
[4] G. Li, et al., Transcriptomic profiling Maps anatomically patterned subpopulations among single embryonic cardiac cells, Dev. Cell 39 (2016) 491–507, https://doi.org/10.1016/j.devcel.2016.10.014.
[5] D.M. DeLaughter, et al., Single-cell resolution of temporal gene expression during heart development, Dev. Cell 39 (2016) 480–490, https://doi.org/10.1016/j.devcel.2016.10.001.
[6] Y. Cui, et al., Single-cell transcriptome analysis Maps the developmental Track of the human heart, Cell Rep. 26 (2019) 1934–1950 e1935, https://doi.org/10.1016/j.celrep.2019.01.079.
[7] M. Asp, et al., A spatiotemporal organ-Wide gene expression and cell Atlas of the developing human heart, Cell 179 (2019) 1647–1660 e1619, https://doi.org/10.1016/j.cell.2019.11.025.
[8] W. Feng, et al., Single-cell transcriptomic analysis identifies murine heart molecular features at embryonic and neonatal stages, Nat. Commun. 13 (2022) 7960, https://doi.org/10.1038/s41467-022-35691-7.
[9] M. Ameen, et al., Integrative single-cell analysis of cardiogenesis identifies developmental trajectories and non-coding mutations in congenital heart disease, Cell 185 (2022) 4937–4953 e4923, https://doi.org/10.1016/j.cell.2022.11.028.
[10] X. Liu, et al., Single-cell RNA-seq of the developing cardiac outflow tract reveals Convergent development of the vascular smooth muscle cells, Cell Rep. 28 (2019) 1346–1361 e1344, https://doi.org/10.1016/j.celrep.2019.06.092.
[11] T.Y. de Soysa, et al., Single-cell analysis of cardiogenesis reveals basis for organ-level developmental defects, Nature 572 (2019) 120–124, https://doi.org/10.1038/s41586-019-1414-x.
[12] L. Wang, et al., Single-cell reconstruction of the adult human heart during heart failure and recovery reveals the cellular landscape underlying cardiac function, Nat. Cell Biol. 22 (2020) 108–119, https://doi.org/10.1038/s41556-019-0446-7.
[13] N. Yamaguchi, et al., An Anterior second heart Field Enhancer regulates the gene regulatory network of the cardiac outflow tract, Circulation 148 (2023) 1705–1722, https://doi.org/10.1161/CIRCULATIONAHA.123.065700.
[14] E.J. Lammer, et al., Retinoic acid embryopathy, N. Engl. J. Med. 313 (1985) 837–841, https://doi.org/10.1056/NEJM198510033131401.
[15] H. Yasui, M. Nakazawa, M. Morishima, S. Miyagawa-Tomita, K. Momma, Morphological observations on the pathogenetic process of transposition of the great arteries induced by retinoic acid in mice, Circulation 91 (1995) 2478–2486, https://doi.org/10.1161/01.cir.91.9.2478.
[16] H. Yasui, M. Morishima, M. Nakazawa, E. Aikawa, Anomalous looping, atrioventricular cushion dysplasia, and unilateral ventricular hypoplasia in the mouse embryos with right isomerism induced by retinoic acid, Anat. Rec. 250 (1998) 210–219, https://doi.org/10.1002/(SICI)1097-0185(199802)250:2<210::AID-AR11>3.0.CO;2-R.
[17] Q. Chu, et al., CACCT: an Automated Tool of detecting Complicated cardiac malformations in mouse models, Adv. Sci. 7 (2020) 1903592, https://doi.org/10.1002/advs.201903592.
[18] M. Shao, L. Wang, Q. Zhang, T. Wang, S. Wang, STMN2 overexpression promotes cell proliferation and EMT in pancreatic cancer mediated by WNT/beta-catenin signaling, Cancer Gene Ther. 30 (2023) 472–480, https://doi.org/10.1038/s41417-022-00568-w.
[19] R.M. Barnes, et al., MEF2C regulates outflow tract alignment and transcriptional control of Tdgf1, Development 143 (2016) 774–779, https://doi.org/10.1242/dev.126383.
[20] K.S. Latacha, et al., Role of actin polymerization in bending of the early heart tube, Dev. Dynam. : an official publication of the American Association of Anatomists 233 (2005) 1272–1286, https://doi.org/10.1002/dvdy.20488.
[21] H. Matsson, et al., Alpha-cardiac actin mutations produce atrial septal defects, Hum. Mol. Genet. 17 (2008) 256–265, https://doi.org/10.1093/hmg/ddm302.
[22] M. Azhar, et al., Ligand-specific function of transforming growth factor beta in epithelial-mesenchymal transition in heart development, Dev. Dynam. : an official publication of the American Association of Anatomists 238 (2009) 431–442, https://doi.org/10.1002/dvdy.21854.
[23] X. Wang, et al., S100A10 promotes HCC development and progression via transfer in extracellular vesicles and regulating their protein cargos, Gut 72 (2023) 1370–1384, https://doi.org/10.1136/gutjnl-2022-327998.
[24] B. Phipson, et al., propeller: testing for differences in cell type proportions in single cell data, Bioinformatics 38 (2022) 4720–4726, https://doi.org/10.1093/bioinformatics/btac582.
[25] J.E. Balmer, R. Blomhoff, Gene expression regulation by retinoic acid, J. Lipid Res. 43 (2002) 1773–1808, https://doi.org/10.1194/jlr.r100015-jlr200.
[26] S.C. Jin, et al., Contribution of rare inherited and de novo variants in 2,871 congenital heart disease probands, Nat. Genet. 49 (2017) 1593–1601, https://doi.org/10.1038/ng.3970.
[27] G.S. Gulati, et al., Single-cell transcriptional diversity is a hallmark of developmental potential, Science 367 (2020) 405–411, https://doi.org/10.1126/science.aax0249.